Hybrid crystals of cuprates and iron-based superconductors*

Xia Dai(代霞)[1], Cong-Cong Le(勒聪聪)[1], Xian-Xin Wu(吴贤新)[1], and Jiang-Ping Hu(胡江平)[1,2,3,†]

[1] *Institute of Physics, Chinese Academy of Sciences, Beijing* 100190, *China*
[2] *Collaborative Innovation Center of Quantum Matter, Beijing, China*
[3] *Department of Physics, Purdue University, West Lafayette, Indiana* 47907, *USA*

(Received 29 January 2016; revised manuscript received 19 April 2016; published online 27 May 2016)

We propose two possible new compounds, $Ba_2CuO_2Fe_2As_2$ and $K_2CuO_2Fe_2Se_2$, which hybridize the building blocks of two high temperature superconductors, cuprates and iron-based superconductors. These compounds consist of square CuO_2 layers and antifluorite-type Fe_2X_2 (X = As, Se) layers separated by Ba/K. The calculations of binding energies and phonon spectra indicate that they are dynamically stable, which ensures that they may be experimentally synthesized. The Fermi surfaces and electronic structures of the two compounds inherit the characteristics of both cuprates and iron-based superconductors. These compounds can be superconductors with intriguing physical properties to help to determine the pairing mechanisms of high T_c superconductivity.

Keywords: iron-based superconductors, cuprates, first-principle calculation

PACS: 74.70.Xa, 61.50.–f, 75.50.Bb, 71.15.Mb **DOI:** 10.1088/1674-1056/25/7/077402

1. Introduction

Cuprates,[1–8] first discovered in 1986, and iron-based superconductors (IBS),[9–13] discovered in early 2008, are two classes of unconventional high temperature superconductors which share many common features. Both of them are quasi-two-dimensional and the phase diagrams are similar in which superconductivity develops after a magnetic order is suppressed.[14–16] All the cuprates share a common structure element CuO_2 plane, where the Cu atoms form a square lattice.[17] The IBS share a common Fe_2X_2 (X = As and Se) layered structure unit, which possesses an anti-PbO-type (anti-litharge-type) atom arrangement. The Fe_2X_2 layers consist of a square lattice sheet of Fe coordinated by X above and below the plane to form face sharing FeX_4 tetrahedra.[18]

One of the major questions in the field of high T_c superconductors is whether cuprates and IBS share a common superconducting mechanism.[16,19] The answer to this question may be obtained if we can integrate the characteristics of both superconductors into a single compound so that their relations can be exclusively addressed. As both structures are featured with layered square lattices with similar in-plane lattice constants, it is possible to design a compound containing both building blocks, Cu–O layers of cuprates and Fe–As(Se) layers of IBS. Similar material designs have been adopted[20,21] and a target material $Nd_4CuO_6Fe_2As_2$ has been theoretically investigated.[20]

Recently, two new materials $Ba_2MO_2Ag_2Se_2$ (M = Co, Mn)[22] have been synthesized via a solid-state reaction in experiment. These two compounds, whose structures belong to the $I4/mmm$ space group, consist of infinite MO_2 square planes and antifluorite-type Ag_2Se_2 layers separated by barium. In this paper, motivated by the fact that the MO_2 plane resembles the CuO_2 plane in cuprates and the Ag_2Se_2 layer resembles the Fe_2X_2 layer in IBS, we consider the substitution of Cu and Fe for M and Ag in the compounds respectively to obtain two possible new compounds, $Ba_2CuO_2Fe_2As_2$ and $K_2CuO_2Fe_2Se_2$. Similar structures have been realized in $Sr_2CrO_2A_2As_2$ (A = Fe, Cr).[23,24] We perform density functional calculations to study the stability and basic electronic structures of these new compounds. We find that these materials integrate basic electronic characteristics of both high T_c superconductors. In $Ba_2CuO_2Fe_2As_2$, the CuO_2 layers are electron-doped while the Fe_2As_2 layers are hole-doped. The situation is reversed in $K_2CuO_2Fe_2Se_2$. Such doping configurations suggest that many possible mixed phases, in particular, magnetic and superconducting phases, may be realized in these materials by introducing additional carriers and applying an external pressure.

2. Computational details

Our calculations are performed using density functional theory (DFT) employing the projector augmented wave (PAW) method encoded in the Vienna *ab initio* simulation package (VASP).[25–27] Both the local density approximation (LDA) and the generalized-gradient approximation (GGA)[28] for the exchange–correlation functional are used. Throughout the work, the cutoff energy is set to be 500 eV for expanding the wave functions into the plane-wave basis. In the calculations

*Project supported by the National Basic Research Program of China (Grant No. 2015CB921300), the National Natural Science Foundation of China (Grant Nos. 1190020 and 11334012), and the Strategic Priority Research Program of Chinese Academy of Sciences (Grant No. XDB07000000).

†Corresponding author. E-mail: jphu@iphy.ac.cn

© 2016 Chinese Physical Society and IOP Publishing Ltd

of magnetic properties, the LDA + U method is used with the effective on-site Coulomb U being 7 eV for Cu 3d states.[29] In the calculations, the Brillouin zone is sampled in the k space within the Monkhorst–Pcak scheme.[30] The number of these k points depends on the lattice: $15 \times 15 \times 3$ for the general unit cell with 4 Fe atoms and 2 Cu atoms and $9 \times 9 \times 3$ for the $\sqrt{2} \times \sqrt{2}$ unit cell. We relax the lattice constants and internal atomic positions with both LDA and GGA, where the forces are minimized to less than 0.01 eV/Å. The phonon dispersions are calculated using the finite displacement method[31] as implemented in the PHONOPY code.[32,33]

3. Crystal structure

$Ba_2CuO_2Fe_2As_2$ and $K_2CuO_2Fe_2Se_2$ crystallize in a body-centered tetragonal lattice, as shown in Fig. 1. The Ba (K) spacer layer separates the tetrahedral Fe_2As_2 (Fe_2Se_2) layers and the square CuO_2 layers. There are double Fe_2X_2 (X = As and Se) and CuO_2 layers in a unit cell, similar to $BaFe_2As_2$. In order to predict the structures of $Ba_2CuO_2Fe_2As_2$ and $K_2CuO_2Fe_2Se_2$, the lattices are fully optimized based on the experimental structural parameters of $Ba_2CoO_2Ag_2Se_2$. The optimized and experimental structural parameters are summarized in Table 1. Both of the calculated lattice constants using LDA and GGA are close to those of $Ba_2CoO_2Ag_2Se_2$ in experiment, which validates the adopted substitution. As the calculated lattice parameters for $Ba_2CoO_2Ag_2Se_2$ using GGA are closer to the experimental data, we perform the following calculations for the two materials using the lattice parameters obtained by relaxation with GGA.

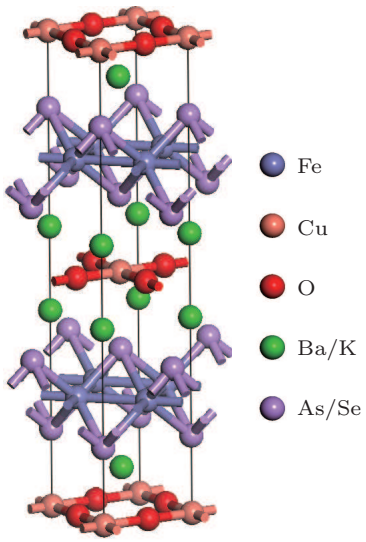


Fig. 1. (color online) Crystal structure of $Ba_2CuO_2Fe_2As_2$ ($K_2CuO_2Fe_2Se_2$).

The binding energy is usually calculated to estimate the stability of new structures. Here, the binding energy per atom, E_b, is defined as $E_b = (4E_{Ba/K} + 2E_{Cu} + 4E_O + 4E_{Fe} + 4E_{As/Se} - E_{total})/18$, where E_{Ba}, E_K, E_{Cu}, E_O, E_{Fe}, E_{As}, and E_{Se} are the respective energies per atom of elemental Ba, K, Cu, O, Fe, As, and Se in the states at room temperature and ambient pressure, and E_{total} is the calculated total energy of a unit cell of $Ba_2CuO_2Fe_2As_2$ ($K_2CuO_2Fe_2Se_2$). The obtained binding energies are 1.61 eV and 1.23 eV per atom for $Ba_2CuO_2Fe_2As_2$ and $K_2CuO_2Fe_2Se_2$, respectively. Both of the binding energies are very close to that of $Ba_2CoO_2Ag_2Se_2$ (1.318 eV), indicating that the two structures are energetically favorable in experiment and may be synthesized using similar methods. To further test the stability of these two structures, we calculate their phonon dispersions, as shown in Fig. 2. No imaginary frequencies are observed throughout the whole Brillouin zone in the phonon dispersions, confirming their dynamically structural stability.

Table 1. Optimized structural parameters of $Ba_2CuO_2Fe_2As_2$ and $K_2CuO_2Fe_2Se_2$ using LDA and GGA in the paramagnetic phase. The 6th column shows the experimental structural parameters of $Ba_2CoO_2Ag_2Se_2$.[22]

	$Ba_2CuO_2Fe_2As_2$		$K_2CuO_2Fe_2Se_2$		$Ba_2CoO_2Ag_2Se_2$
	LDA	GGA	LDA	GGA	Expt.
a/Å	3.902	4.026	3.769	3.839	4.223
c/Å	19.867	20.273	18.320	22.165	20.036

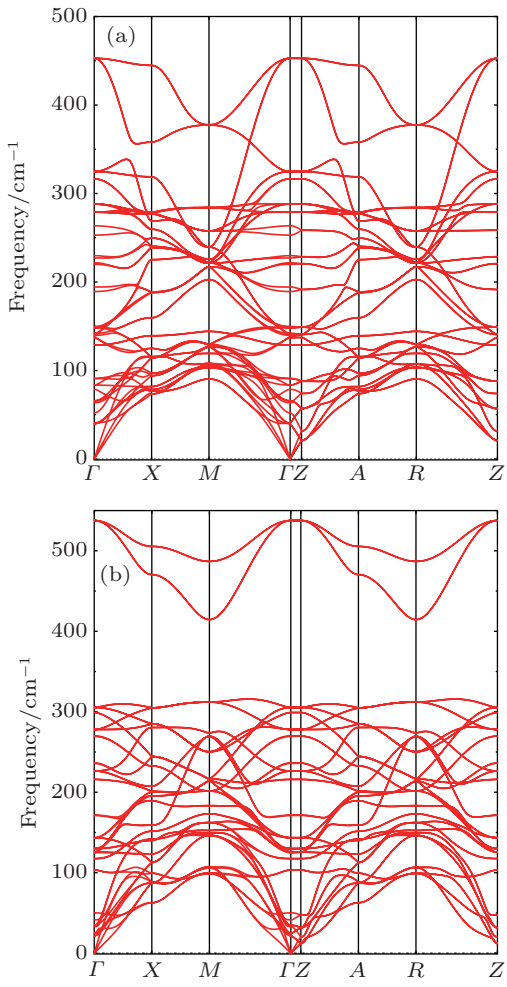


Fig. 2. (color online) Calculated GGA phonon dispersions of (a) $Ba_2CuO_2Fe_2As_2$ and (b) $K_2CuO_2Fe_2Se_2$ in the paramagnetic state.

4. Electronic and magnetic properties

The optimized parameter a of $Ba_2CuO_2Fe_2As_2$ is determined to be 4.026 Å, slightly larger than those of cuprates (3.78 Å for $La_{1.8}Sr_{0.2}CuO_4$[3] and 3.859 Å for $YBa_2Cu_3O_{6+x}$[4]). Compared with three typical kinds of iron pnictides, LiFeAs,[10] $BaFe_2As_2$,[11] and LaFeAsO,[9] as shown in Table 2, the parameter a is very close to those of $BaFe_2As_2$ and LaFeAsO but deviates a little from that of LiFeAs. The obtained As height above the Fe plane in $Ba_2CuO_2Fe_2As_2$ is smaller than those of iron pnictides in experiment. This underestimation has been noted in the study of IBS.[34–36] The Fe_2As_2 inter-layer distance is much larger than the values in the three families of iron pnictides, indicating that it is more two-dimensional than the conventional iron pnictides. The separation between Fe_2As_2 and CuO_2 layers is about 5 Å, which suggests couplings between these layers.

Table 2. Optimized structural parameters of $Ba_2CuO_2Fe_2As_2$ using GGA in the paramagnetic phase and those of LiFeAs,[10] $BaFe_2As_2$,[11] and LaFeAsO.[9] The angle β is the Fe–As–Fe bonding angle of two next nearest Fe atoms.

	$Ba_2CuO_2Fe_2As_2$	LiFeAs	$BaFe_2As_2$	LaFeAsO
a/Å	4.026	3.791	3.963	4.035
β/(°)	118.7	103.1	111.0	113.5
h(Fe–As)/Å	1.19	1.51	1.36	1.32
h(Fe–Fe)/Å	10.14	6.36	6.51	8.74

The band structure and density of states (DOS) for $Ba_2CuO_2Fe_2As_2$ with the GGA optimized structural parameters in the paramagnetic states are shown in Fig. 3. The band structure near the Fermi level resembles those of both typical iron pnictides LaFeAsO[37] and cuprates[14] where Fe 3d states (d_{xz}, d_{yz}, $d_{x^2-y^2}$ orbitals) and Cu 3d states ($d_{x^2-y^2}$ orbitals) dominate the Fermi level. Similar to iron pnictides, it is a bad metal with a low carrier density. The 3d states of Fe are mainly located near the Fermi level from −2.5 eV to 3.0 eV and a pseudogap appears at an electron count of six. The As p states mainly lie 2.5 eV below the Fermi level but slightly mix with the Fe 3d states in the energy range from −1.0 eV to 1.0 eV. The Cu 3d contribution is concentrated between −3.0 eV and 1.5 eV. The O p states are strongly coupled with the 3d states of Cu in the total energy range. The spacer layer Ba 5d and 6s states, which donate electrons to the Fe_2As_2 and CuO_2 layers, are empty and lie 2 eV above the Fermi level. At the Fermi level, the total DOS shows the same negative slope with the minimum slightly above the Fermi level, similar to the conventional IBS within DFT. The DOS at the Fermi energy is about 7.81 eV^{-1}/f.u. for both spins. Considering that there are two Fe atoms in one formula unit for $Ba_2CuO_2Fe_2As_2$ but only one for LaFeAsO, this value (3.91 eV^{-1}/Fe) is larger than that of LaFeAsO (2.62 eV^{-1}/f.u.[37]). The corresponding Pauli susceptibility and specific heat coefficient are $\chi_0 = 2.53 \times 10^{-4}$ emu/mol and $\gamma = 18.4$ mJ/(K^2·mol).

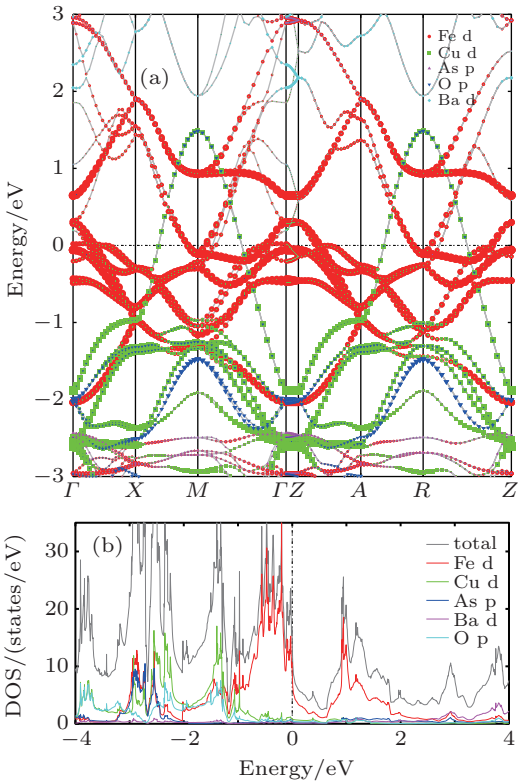


Fig. 3. (color online) (a) Band structures and (b) projected density of states of $Ba_2CuO_2Fe_2As_2$ using the GGA relaxed parameters in the paramagnetic state.

The calculated Fermi surfaces of $Ba_2CuO_2Fe_2As_2$ are given in Fig. 4, which are very similar to those of both iron pnictides and cuprates. From Fig. 3(a), we find that the Fe d_{xz} and d_{yz} states yield two hole cylinders at the zone center. There is an additional heavy three-dimensional (3D) hole pocket centered at the Γ point, which intersects and anticrosses with the hole cylinders. The 3D pocket is derived from Fe d_{z^2} states which hybridize with As p_z states. At the zone corner, there are two 2D small electron pockets and one 2D large hole pocket. The electron pockets are mainly attributed to Fe d_{xz}, d_{yz}, and $d_{x^2-y^2}$ orbitals (d_{xy} orbitals in the usual Fe lattice). The hole pocket around the M point, however, is mainly derived from Cu $d_{x^2-y^2}$ and O p_x and p_y states, in accordance with the Fermi surfaces of cuprates.[14] All of the Fermi surface sheets are double degenerate as there are two Fe_2As_2 and CuO_2 layers in one unit cell.

It is interesting to see that the hole pockets at the Γ point are large, which indicates heavy hole doping in the Fe_2As_2 layers. From the size of the pockets, we can estimate that the hole doping concentration with respect to $BaFe_2As_2$ is roughly 0.15 holes per Fe atom. Considering the hole doping level, the Fermi surfaces attributed to the Fe_2As_2 layers should be similar to those of $Ba_{0.7}K_{0.3}Fe_2As_2$ except that the pockets here are much more two-dimensional. This hole doping level is very close to that in optimally-hole-doped pnictide $Ba_{0.6}K_{0.4}Fe_2As_2$,[38–40] where T_c can reach 37 K. Actually, the calculated Fermi surfaces are similar to those of (Ba,

K)Fe_2As_2 obtained in the ARPES experiment.[41,42] As required by the charge conservation, the heavy hole doping in the Fe_2As_2 layers suggests that the CuO_2 layers must be heavily electron-doped with the same doping concentration. This consistency is confirmed by the estimation that the size of the largest hole pocket at the M point attributed to $d_{x^2-y^2}$ orbitals in CuO_2 layers is about 0.3 electrons per Cu atom from their half filling configuration. The doping level is a little far away from the narrow superconducting region for electron-doped cuprates in the phase diagram.[14]

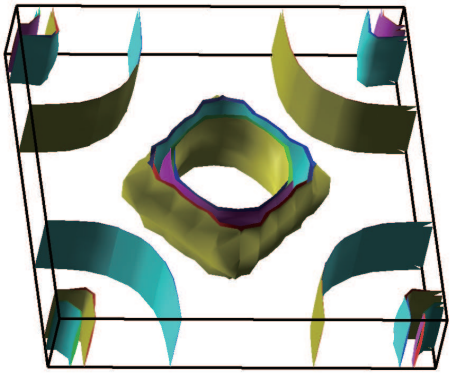


Fig. 4. (color online) Calculated Fermi surfaces of $Ba_2CuO_2Fe_2As_2$ using the GGA relaxed parameters in the paramagnetic state.

The superconductivity in both cuprates and IBS is most likely related to the magnetism. Therefore, we investigate the magnetic properties of this new compound. With such a large doping in the Fe_2As_2 and CuO_2 layers, it is expected that the checkboard antiferromagnetic (AFM) order in the CuO_2 layers and the E-type collinear AFM order in the Fe_2As_2 layers should be significantly weakened or completely suppressed even in the meanfield type of DFT calculations. To check this, we consider four possible magnetic states for Fe_2As_2 and CuO_2 layers: paramagnetic state, ferromagnetic state, checkerboard AFM state, and collinear AFM state. We calculate the total energies of these magnetic states using the LDA + U approach. The calculations show that there is no statically ordered moment in the CuO_2 layers while the E-type collinear AFM order in the Fe_2As_2 layers is still possible. We find that in the DFT result, the E-type state has an energy gain of 103.5 meV/f.u. relative to the paramagnetic state and a spin moment of 1.59 μ_B for each Fe. It is known that magnetic moments calculated for the known parent compounds of IBS, for example, $BaFe_2As_2$, are typically over 2.0 μ_B.[36,43] This moment value is significantly lowered, which is consistent with our expectation as the Fe_2As_2 layers are overdoped by holes. Figures 5(a) and 5(b) show the calculated band structure and DOS in the E-type collinear AFM state (with $\sqrt{2}\times\sqrt{2}$ supercell) with internal coordinates fixed to the values obtained by non-spin-polarized energy minimization. The E-type state is still metallic with a low carrier concentration and $N(E_F)$ decreases severely. Among the considered magnetic states above, the checkerboard AFM state in Fe_2As_2 layers is found to be a metastable state relative to the E-type collinear AFM state. The energy gain is 81.5 meV/f.u. relative to the paramagnetic state and the magnetic moment is about 1.58 μ_B for each Fe atom.

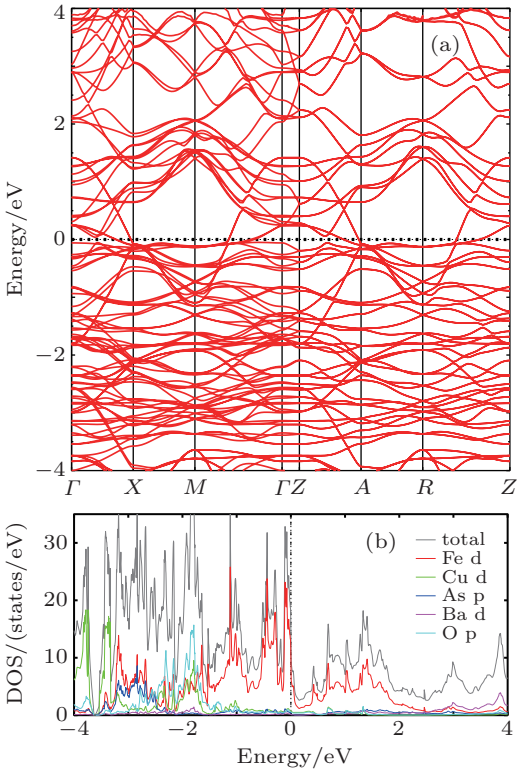


Fig. 5. (color online) (a) Band structures and (b) projected density of states of $Ba_2CuO_2Fe_2As_2$ using the GGA relaxed parameters in the E-type collinear AFM state.

With the substitution of As by Se and Ba by K in $Ba_2CuO_2Fe_2As_2$, we obtain a new compound $K_2CuO_2Fe_2Se_2$. Compared with $Ba_2CuO_2Fe_2As_2$, the parameter a decreases to 3.839 Å but c increases to 22.165 Å, which is consistent with those of iron chalcogenides. Table 3 lists the calculated lattice parameters using GGA and those of KFe_2Se_2[13] and FeSe.[44] The calculated Se height and Se–Fe–Se bond angle are very close to those of FeSe, indicating that they may share some common electronic and magnetic properties. The Se heights are severely underestimated in the calculations compared with those in experiment.[45] The band structure and DOS are shown in Fig. 6. The band structure is similar to that of $Ba_2CuO_2Fe_2As_2$. The DOS between −2.5 eV and 2.0 eV is dominated by Fe 3d states, and Se 3p states are mainly located at 3.5 eV below the Fermi level. The Cu 3d states and O 2p states are strongly coupled from −4.0 eV to 2.5 eV. The K atoms have no contribution to the bands near the Fermi level. To analyze the orbital characters near the Fermi level, we plot the fat band in Fig. 6(a). The DOS at the Fermi level is 4.54 eV^{-1}/f.u., which is significantly lower than that of $Ba_2CuO_2Fe_2As_2$. The corresponding Pauli susceptibility and

specific heat coefficient are $\chi_0 = 1.47 \times 10^{-4}$ emu/mol and $\gamma = 10.7$ mJ/(K^2·mol). Figure 7 shows the calculated Fermi surfaces. The Fermi surfaces are two-dimensional cylinders. The Fe 3d states yield two hole pockets at the Γ point and two small electron pockets at the M point. The hole pockets are attributed to the d_{xz} and d_{yz} states while the electron pockets are derived from Fe d_{xz}, d_{yz}, and $d_{x^2-y^2}$ states. The Fermi surfaces are similar to those in KFe_2Se_2 where hole pockets are absent.[46] Besides the pockets from the Fe_2Se_2 layers, there are additional two hole pockets around the Brillouin zone corners. The bigger pocket is mainly contributed from the Cu $d_{x^2-y^2}$ states, which are strongly coupled with the O p_x and p_y states, while the smaller one is derived from the O p_x and p_y states. All of the Fermi surface sheets are double degenerate just like those in $Ba_2CuO_2Fe_2As_2$.

Table 3. Optimized structural parameters of $K_2CuO_2Fe_2Se_2$ using GGA in the paramagnetic phases and those of KFe_2Se_2[13] and FeSe.[44] The angle β is the Fe–Se–Fe bonding angle of two next nearest Fe atoms.

	$K_2CuO_2Fe_2Se_2$	KFe_2Se_2	FeSe
a/Å	3.839	3.913	3.765
β/(°)	111.6	106.6	111.3
h(Fe–Se)/Å	1.31	1.46	1.29
h(Fe–Fe)/Å	11.08	7.02	5.52

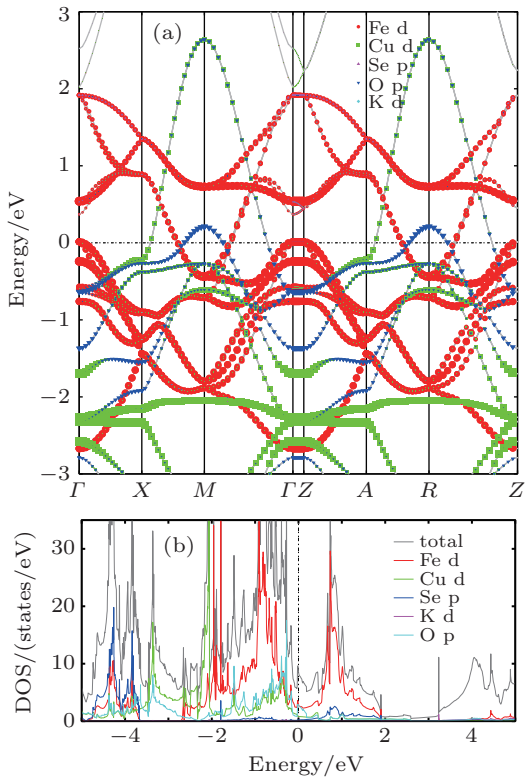


Fig. 6. (color online) (a) Band structures and (b) projected density of states of $K_2CuO_2Fe_2Se_2$ using the GGA relaxed parameters in the paramagnetic state.

Compared with the Fermi surfaces of $Ba_2CuO_2Fe_2As_2$, we find that the hole pockets at the Γ point of $K_2CuO_2Fe_2Se_2$ are much smaller while the electron pockets at the M point are much larger (see Fig. 7), which indicate heavy electron doping in the Fe_2Se_2 layer. From the size of the pockets, we can estimate that the electron doping concentration with respect to FeSe is roughly 0.16 electrons per Fe atom. Similarly, we can check the consistency required by the charge conservation. The size of the hole pockets at the M point from the CuO_2 layers is about 0.32 holes for each CuO_2 layer from their half filling configuration.

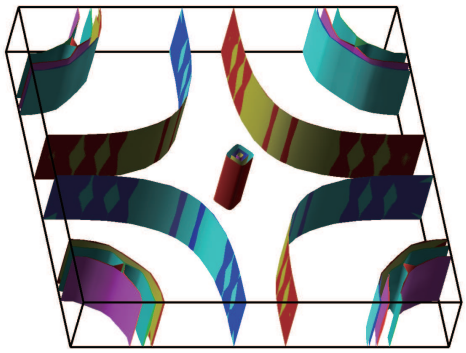


Fig. 7. (color online) Calculated Fermi surfaces of $K_2CuO_2Fe_2Se_2$ using the GGA relaxed parameters in the paramagnetic state.

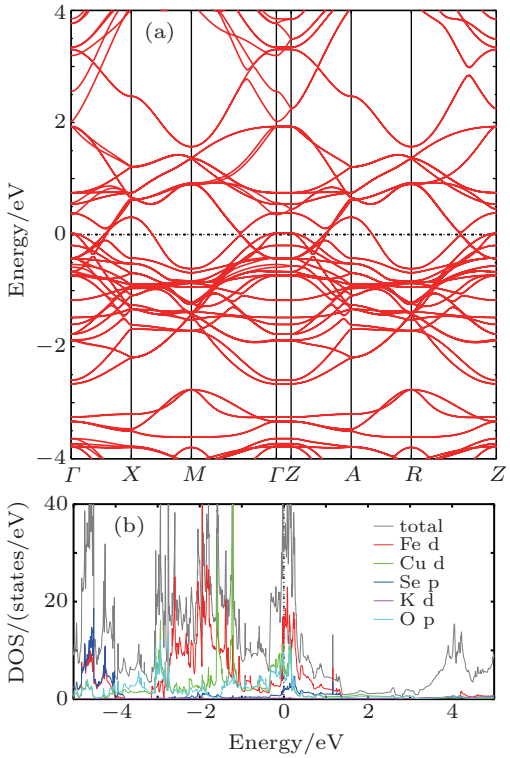


Fig. 8. (color online) (a) Band structures and (b) projected density of states of $K_2CuO_2Fe_2Se_2$ using the GGA relaxed parameters in the AFM state.

The DOS at the Fermi level attributed to Fe 3d orbitals is significantly decreased with such a large electron doping, which may suggest that the magnetic order in the Fe_2Se_2 layers is strongly suppressed. Compared with $Ba_2CuO_2Fe_2As_2$, we consider an additional bicollinear magnetic state, which is the ground state in FeTe.[47] The ground state is paramagnetic

on Fe_2Se_2 layers and checkboard AFM ordered for CuO_2 layers with an energy gain of 196.0 meV/f.u. and a spin moment of 0.59 μ_B per Cu. The band structure and DOS are shown in Fig. 8 and the system remains metallic. In this case, the Fe 3d, Cu 3d, and O 2p states dominate the Fermi level. The DOS at the Fermi level is 7.04 eV^{-1}/f.u. for the spin up channel.

5. Discussion

It is well known that the pairing symmetry is d-wave for the cuprates and s-wave for the iron pnictides with a potential sign change between the hole and electron Fermi pockets. As the proposed new materials contain both CuO_2 layers and Fe_2X_2 (X = As, Se) layers and the electronic structures are similar to both, it can be expected that two different pairing symmetries may coexist in a single material. The proximity effect between two types of layers with different pairing symmetries can result in interesting novel phenomena. The time reversal symmetry may be broken with mixed s-wave and d-wave pairing symmetries.

Introducing additional carriers or applying an external pressure to these materials can maximize T_c. For $Ba_2CuO_2Fe_2As_2$, the doping of the Fe_2As_2 layer is 0.15 holes per Fe and that of CuO_2 is 0.3 electrons per Cu. The doping for the Fe_2As_2 layer is near the optimal level but that for the CuO_2 layer is unfortunately not in the superconducting region. To realize superconductivity for both layers, we can introduce hole doping with partial replacement of Ba^{2+} ions by K^+ ions. From the phase diagrams of cuprates and (Ba,K)Fe_2As_2, the above case can be realized in $Ba_{2-x}K_xCuO_2Fe_2As_2$ ($0.24 \leq x \leq 0.32$) by assuming that the Fe_2As_2 and CuO_2 layers are equally hole doped. In this doping region, the T_c for the Fe_2As_2 layers shows little change. The $x = 0.3$ corresponds the optimal doping value for the electron-doped cuprates.[14] For $K_2CuO_2Fe_2Se_2$, however, the Fe_2Se_2 layers are electron doped and the hole doping for the CuO_2 layers is not in the superconducting region but very close to it. The superconductivity for both layers can be realized in $K_{2-x}Ba_xCuO_2Fe_2Se_2$ ($0.10 \leq x \leq 0.54$). This doping region is much wider than that in $Ba_2CuO_2Fe_2As_2$ due to the wide hole-doped superconducting region in cuprates. The optimal doping value for the CuO_2 layers is $x = 0.34$. The pressure is also an effective way to tune the superconductivity.

6. Conclusion

In conclusion, we identify two hypothetical compounds $Ba_2CuO_2Fe_2As_2$ and $K_2CuO_2Fe_2Se_2$ containing Fe_2X_2 layers and CuO_2 layers, which are the basic structural units of IBS and cuprates, respectively. The metallic spacer Ba (K) separates the basic units. The calculations of binding energies and phonon spectra indicate that they are dynamically stable, ensuring that they may be experimentally synthesized. The Fermi surfaces derived from Fe_2As_2(Fe_2Se_2) layers and CuO_2 layers are very similar to those of iron pnictides (iron chalcogenides) and cuprates, respectively. With heavy self-doping, the ground state of $Ba_2CuO_2Fe_2As_2$ is determined to be an E-type collinear AFM state in the Fe_2As_2 layer and a paramagnetic state in the CuO_2 layer, while $K_2CuO_2Fe_2Se_2$ favors a checkboard AFM state in the CuO_2 layers and a paramagnetic state in the Fe_2Se_2 layers. Without external doping, superconductivity can only be achieved in the Fe_2X_2 layers. However, with external doping through substitution, superconductivity for both Fe_2X_2 and CuO_2 layers can be simultaneously achieved in $Ba_{2-x}K_xCuO_2Fe_2As_2$ ($0.24 \leq x \leq 0.32$) and $K_{2-x}Ba_xCuO_2Fe_2Se_2$ ($0.10 \leq x \leq 0.54$). The synthesis of these new compounds will not only provide us with a unique opportunity to explore exotic properties in cuprates and IBS simultaneously but also help us to understand the mechanism of high T_c superconductivity.

References

[1] Bednorz J G and Muller K A 1986 *Z. Phys. B* **64** 189
[2] Kishio K, Kitazawa K, Kanbe S, Yasuda I, Sugii N, Takagi H, Uchida S, Fueki K and Tanaka S 1987 *Chem. Lett.* **16** 429
[3] Cava R J, Dover R B, Batlogg B and Rietman E A 1987 *Phys. Rev. Lett.* **58** 408
[4] Hazen R M, Finger L W, Angel R J, Prewitt C T, Ross N L, Mao H K and Hadidiacos C G 1987 *Phys. Rev. B* **35** 7238
[5] Wu M K, Ashburn J R, Torng C J, Hor P H, Meng R L, Gao L, Huang Z J, Wang Y Q and Chu C W 1987 *Phys. Rev. Lett.* **58** 908
[6] Maeda H, Tanaka Y, Fukutomi M and Asano T 1988 *Jpn. J. Appl. Phys.* **27** L209
[7] Sheng Z Z and Hermann A M 1988 *Nature* **332** 55
[8] Schilling A, Cantoni M, Guo J D and Ott H R 1993 *Nature* **363** 56
[9] Kamihara Y, Watanabe T, Hirano M and Hosnon H 2008 *J. Am. Chem. Soc.* **130** 3296
[10] Tapp J H, Tang Z, Lv B, Sasmal K, Lorenz B, Chu P C W and Guloy A M 2008 *Phys. Rev. B* **78** 060505
[11] Rotter M, Tegel M, Johrendt D, Schellenberg I, Hermes W and Pottgen R 2008 *Phys. Rev. B* **78** 020503
[12] Hsu F C, Luo J Y, Yeh K W, Chen T K, Huang T W, Wu P M, Lee Y C, Huang Y L, Chu Y Y, Yan D C and Wu M K 2008 *Proc. Natl. Acad. Sci. USA* **105** 14262
[13] Guo J G, Jin S F, Wang G, Wang S C, Zhu K X, Zhou T T, He M and Chen X L 2010 *Phys. Rev. B* **82** 180520
[14] Damascelli A, Hussain Z and Shen Z X 2003 *Rev. Mod. Phys.* **75** 473
[15] Basov D N and Chubukov A V 2011 *Nat. Phys.* **7** 272
[16] Hu J P and Ding H 2012 *Sci. Rep.* **2** 381
[17] Barisic N, Chan M K, Li Y, Yu G, Zhao X, Dressel M, Smontara A and Greven M 2013 *Proc. Natl. Acad. Sci. USA* **110** 12235
[18] Paglione J and Greene R L 2010 *Nat. Phys.* **6** 645
[19] Scalapino D J 2012 *Rev. Mod. Phys.* **84** 1383
[20] Ricci A, Joseph B, Poccia N, Xu W, Chen D, Chu W S, Wu Z Y, Marcelli A, Saini N L and Bianconi A 2010 *Supercond. Sci. Technol.* **23** 052003
[21] Jiang H, Sun Y L, Xu Z A and Cao G H 2013 *Chin. Phys. B* **22** 087410
[22] Zhou T T, Wang Y M, Jin S F, Li D D, Lai S F, Ying T P, Zhang H, Shen S J, Wang W J and Chen X L 2014 *Inorg. Chem.* **53** 4154
[23] Eguchi N, Ishikawa F, Kodama M, Wakabayashi T, Nakayama A, Ohmura A and Yamada Y 2013 *J. Phys. Soc. Jpn.* **82** 045002
[24] Jiang H, Bao J K, Zhai H F, Tang Z T, Sun Y L, Liu Y, Wang Z C, Bai H, Xu Z A and Cao G H 2015 *Phys. Rev. B* **92** 205107
[25] Kresse G and Hafner J 1993 *Phys. Rev. B* **47** 558
[26] Kresse G and Furthmuller J 1996 *Comput. Mater. Sci.* **6** 15
[27] Kresse G and Furthmuller J 1996 *Phys. Rev. B* **54** 11169
[28] Perdew J P, Burke K and Ernzerhof M 1996 *Phys. Rev. Lett.* **77** 3865
[29] Czyzyk M T and Sawatzky G A 1994 *Phys. Rev. B* **49** 14211

[30] Monkhorst H J and Pack J 1976 *Phys. Rev. B* **13** 5188
[31] Alfe D 2009 *Computer Physics Communications* **180** 2622
[32] Togo A, Oba F and Tanaka I 2008 *Phys. Rev. B* **78** 134106
[33] Togo A and Tanaka I 2015 *Scr. Mater.* **108** 1
[34] Yin Z P, Lebegue S, Han M J, Neal B P, Savrasov S Y and Pickett W E 2008 *Phys. Rev. Lett.* **101** 047001
[35] Mazin I I, Johannes M D, Boeri L, Koepernik K and Singh D J 2008 *Phys. Rev. B* **78** 085104
[36] Singh D J 2008 *Phys. Rev. B* **78** 094511
[37] Singh D J and Du M H 2008 *Phys. Rev. Lett.* **100** 237003
[38] Ding H, Richard P, Nakayama K, Sugawara T, Arakane T, Sekiba Y, Takayama A, Souma S, Sato T, Takahashi T, Wang Z, Dai X, Fang Z, Chen G F, Luo J L and Wang N L 2008 *Europhys. Lett.* **83** 47001
[39] Zhao L, Liu H Y, Zhang W T, Meng J Q, Jia X W, Liu G D, Dong X L, Chen G F, Luo J L, Wang N L, Wang G L, Zhou Y, Zhu Y, Wang X Y, Zhao Z X, Xu Z Y, Chen C T and Zhou X J 2008 *Chin. Phys. Lett.* **25** 4402
[40] Nakayama K, Sato T, Richard P, Xu Y M, Sekiba Y, Souma S, Chen G F, Luo J L, Wang N L, Ding H and Takahashi T 2009 *Europhys. Lett.* **85** 67002
[41] Liu C, Samolyuk G D, Lee Y, Ni N, Kondo T, Santander-Syro A F, Budko S L, McChesney J L, Rotenberg E, Valla T, Fedorov A V, Canfield P C, Harmon B N and Kaminski A 2008 *Phys. Rev. Lett.* **101** 177005
[42] Xu Y M, Richard P, Nakayama K, Kawahara T, Sekiba Y, Qian T, Neupane M, Souma S, Sato T, Takahashi T, Luo H Q, Wen H H, Chen G F, Wang N L, Wang Z, Fang Z, Dai X and Ding H 2011 *Nat. Commun.* **2** 392
[43] Akturk E and Ciraci S 2009 *Phys. Rev. B* **79** 184523
[44] Subedi A, Zhang L, Singh D J and Du M H 2008 *Phys. Rev. B* **78** 134514
[45] Lehman M C, Llobet A, Horigane K and Louca D 2010 *J. Phys.: Conf. Ser.* **251** 012009
[46] Zhang Y, Yang L X, Xu M, Ye Z R, Chen F, He C, Xu H C, Jiang J, Xie B P, Ying J J, Wang X F, Chen X H, Hu J P, Matsunami M, Kimura S and Feng D L 2011 *Nat. Mater.* **10** 273
[47] Ma F J, Ji W, Hu J P, Lu Z Y and Xiang T 2009 *Phys. Rev. Lett.* **102** 177003